Correspondence to:

X. Li,
lixw39@mail.sysu.edu.cn

Reducing the Spring Barrier in Predicting Summer Arctic Sea Ice Concentration

Jingwen Zeng[1] [iD], **Qinghua Yang[1]** [iD], **Xuewei Li[1]** [iD], **Xiaojun Yuan[2]** [iD], **Mitchell Bushuk[3]** [iD], and **Dake Chen[1]** [iD]

[1]School of Atmospheric Sciences, Sun Yat-sen University, and Southern Marine Science and Engineering Guangdong Laboratory (Zhuhai), Zhuhai, China, [2]Lamont-Doherty Earth Observatory, Columbia University, Palisades, NY, USA, [3]Geophysical Fluid Dynamics Laboratory, Princeton, NJ, USA

Abstract The predictive skill of summer sea ice concentration (SIC) in the Arctic presents a steep decline when initialized before June, which is the so-called spring predictability barrier for Arctic sea ice. This study explores the potential influence of surface heat flux, cloud and water vapor anomalies on monthly to seasonal predictions of Arctic SIC anomalies. The results show an enhancement in skill predicting Arctic September SIC in the models that use surface fluxes, clouds, or water vapor in combination with SIC and surface sea temperature as predictors when initialized in boreal spring. This result shows the potential to reduce the spring barrier for Arctic SIC predictions by including the surface heat budget. The enhanced predictive skill can be very likely linked to the improved representation of the thermodynamics associated with water vapor and cloudiness anomalies in spring.

Plain Language Summary Under the influence of climate change, the summer sea ice extent in the Arctic presents significant variability and thus is crucial to human activities in the Arctic. However, the predictive skill for summer sea ice in the Arctic shows a steep decline when predictions are initiated before June, which is called the spring barrier. In this study, we show that adding surface heat fluxes (net surface heat flux, net surface long wave radiation and net surface shortwave radiation), clouds or water vapor into a statistical prediction model can better represent the interactive processes at the atmosphere and ocean interface. The enhancement improves the predictive skill of summer sea ice in the Arctic and reduces the spring barrier, especially in areas of the Beaufort Sea, Chukchi Sea, and Central Arctic.

1. Introduction

Under the influence of climate change, the Arctic has warmed at least twice the rate of global warming (Ballinger et al., 2020; Rantanen et al., 2022) There has been a corresponding rapid decrease of summer sea ice concentration (SIC) in the seasonal ice area, along with a retreat of Arctic summer sea ice extent, decreasing at a rate of around 13% per decade (Perovich et al., 2020). Consequently, chances have arisen for increased economic and conservation activity in the Arctic, which urges for more precise predictions of Arctic SIC (e.g., Emmerson & Lahn, 2012; Jung et al., 2016; Melia et al., 2016).

The prediction of Arctic SIC largely depends on the initial state of SIC itself and the influence of thermodynamic and dynamic processes (Bushuk et al., 2020; Guemas et al., 2014). However, the predictive skill of summer SIC presents a steep decline when initialized before June, which can be regarded as an "Arctic spring predictability barrier." The timing of the barrier is defined by a significant rise in predictability, attributed to melt-generated SIM anomalies that emerge at the onset of the melting process (Bonan et al., 2019; Bushuk et al., 2020). The spring barrier has been confirmed in both dynamical and statistical prediction models (Bonan et al., 2019; Lindsay et al., 2008a; Sigmond et al., 2013; Stroeve et al., 2014). Among statistical models, linear regression models and linear Markov models are the most commonly used (Brunette et al., 2019; Chen & Yuan, 2004; Drobot & Maslanik, 2002; M.-L. Kapsch et al., 2014; Lenetsky et al., 2021; Lindsay et al., 2008b; Onarheim et al., 2015; Petty et al., 2017; Schröder et al., 2014; Walsh et al., 2019; Wang et al., 2016; Williams et al., 2016; Yuan et al., 2016). Linear Markov models that incorporate atmospheric and oceanic conditions have been found to skillfully predict Arctic SIC (Chen & Yuan, 2004a; Drobot & Maslanik, 2002; L. Wang et al., 2016; Yuan et al., 2016). Wang, Yuan, Bi, et al. (2022) and Wang, Yuan, & Cane (2022) found that upper ocean heat content and SAT provide more predictive skill for summer SIC in the

Writing – review & editing: Qinghua Yang, Xuewei Li, Xiaojun Yuan, Mitchell Bushuk, Dake Chen

Pacific sector of the Arctic than other combinations of predictors in a linear Markov model. Yuan et al. (2016) found that, compared with dynamic processes, thermodynamic processes dominated the model skill in most areas.

Several studies have shown that surface fluxes have important influences on sea ice variability through ice-albedo feedback and other thermodynamic processes. Choi et al. (2014) pointed out a significant lagged covariance between absorbed solar radiation in spring to early summer and SIC anomalies in late summer. Kapsch et al. (2014) found that downwelling longwave radiation and vertically integrated water vapor in April and May provided skillful predictions of September SIC. To make seasonal predictions based on data in boreal spring, Drobot (2007) and Liu et al. (2015) considered surface albedo as well as surface downwelling longwave radiation flux and melt pond fraction, respectively. In the Antarctic, cloud anomalies are highly coupled with SIC anomalies in a wave-3 pattern (Wang, Yuan, Bi, et al., 2022; Wang, Yuan, & Cane, 2022). Their results indicate a possibility that surface fluxes may improve predictive skill for forecasts initialized before June. Kapsch et al. (2014) also point out the importance of atmospheric processes in spring to September SIC. Therefore, making use of springtime surface fluxes may improve the predictive skill in statistical models.

In this study, we attempt to address the following scientific question: Can the Arctic spring barrier be reduced in statistical models by considering surface heat fluxes? The paper is organized into four sections. The data and the multivariate linear Markov model are introduced in Section 2. Section 3 introduces the precursory role of surface fluxes in determining the Arctic sea ice concentration in September and the predictive skill of various statistical methods in predicting Arctic SIC. Finally, we summarize and discuss the major findings of this study in Section 4.

2. Data and Methods

2.1. Data

Our control experiment (Ctrl) is based on Yuan et al. (2016), therefore, we use the same data as Yuan et al. (2016): monthly SIC data from the National Snow and Ice Data Center (NSIDC; Comiso, 2017), SST data from Hadley Centre Sea Ice and Sea Surface Temperature (HadISST), and SAT data from NCEP-DOE AMIP-II reanalysis data (Kalnay et al., 1996; Kistler et al., 2001). Furthermore, net surface shortwave radiation (NSSW), net surface longwave radiation (NSLW), total column water vapor (WV) and total column cloud water (CW) data from ERA5 reanalysis data (Hersbach et al., 2020), as well as net surface heat flux (NSHF) calculated from NSSW, NSLW, surface latent heat flux and surface sensible heat flux data (all positive downward) from ERA5 reanalysis data are also used. All the variables are monthly data from 1979 to 2019. The climatological annual cycles have been subtracted at each grid point in all data sets prior to analysis. Note that the linear trend is retained in the input data.

2.2. Multivariate Linear Markov Model

In this study, the Multivariate linear Markov model is used to predict the pan-Arctic SICA which is gridded to a horizontal resolution of approximately 25 km × 25 km, on a polar stereographic projection. In this study, we focus on the existing sea ice area from 1979 to 2019 and refer to these regions as "pan-Arctic" (Figure S1 in Supporting Information S1). The Multivariate linear Markov model is constructed on the MEOF space, with temporal component predicted through linear autoregression, and the prediction of SIC at each grid point is calculated by multiplying the predicted temporal component and spatial component. Statistical models to predict Arctic SIC were constructed from different datasets. The control experiment is the same as the one described in Yuan et al. (2016), which uses SIC, SST and SAT to form the initial multivariate space (described below). In addition, a set of new models (Table 1) were built, in which the weightings among SAT, NSHF, NSSW, NSLW, WV and CW are changed to identify the effects of surface fluxes, cloudiness and water vapor, and the experiments are named by the variables besides SIC and SST (the first left column of Table 1). The weight of SIC is set to be 2 to emphasize the variability of SIC in the construction of the model. The weighted variables are stacked up into a single matrix $\mathbf{V}(p, n)$, where p denotes spatial dimension and n denotes temporal dimension. To reduce the degrees of freedom, we apply multivariate empirical orthogonal function analysis (MEOF) to decompose the matrix $\mathbf{V}(p, n)$ into spatial patterns (eigenvectors) $\mathbf{E}(p, p^*)$ and temporal variability (principal components, PCs) $\mathbf{P}^{\mathrm{T}}(p^*, n)$:

$$\mathbf{V}_{p \times n} = \mathbf{E}_{p \times p^*} \mathbf{P}_{p^* \times n} \tag{1}$$

Table 1
The Weightings Among the Six Variables to Construct Five Sets of the Multivariate Linear Markov Models Used in This Study

EXP	SIC	SST	SAT	NSHF	NSLW	NSSW	WV	CW
Ctrl	2	1	1	0	0	0	0	0
NSHF & SAT	2	1	1	1	0	0	0	0
NSHF	2	1	0	1	0	0	0	0
NSLW	2	1	0	0	1	0	0	0
NSSW	2	1	0	0	0	1	0	0
WV	2	1	0	0	0	0	1	0
CW	2	1	0	0	0	0	0	1

and truncating the first several modes, where p^* denotes the number of modes. The linear Markov model is trained by using EOF-based reconstructions to estimate the transition matrix A of the evolution of the PCs. The transition matrix $\mathbf{A}$ satisfies the following linear relationship:

$$\mathbf{P}_{i+1} = \mathbf{A}\mathbf{P}_i + \mathbf{e}_i \tag{2}$$

where i denotes the ith month in a year and $\mathbf{e}_i$ is the error in the model fit. The transition matrix $\mathbf{A}$ is obtained by multiplying (Equation 2) with $\mathbf{P}_i^T$ and averaging over time, which yields

$$\overline{\mathbf{P}_{i+1}\mathbf{P}_i^T} = \mathbf{A}\overline{\mathbf{P}_i\mathbf{P}_i^T} + \overline{\mathbf{e}_i\mathbf{P}_i^T} \tag{3}$$

$$\mathbf{A}_i = \overline{\mathbf{P}_{i+1}\mathbf{P}_i^T}\left(\overline{\mathbf{P}_i\mathbf{P}_i^T}\right)^{-1} \tag{4}$$

Each calendar month has a corresponding transition matrix A_i. We first compute $\mathbf{A}$ for each calendar month and predict each $\mathbf{P}_{i+1}$ by using the corresponding transition matrix $\mathbf{A}_i$. Then we reconstruct the SIC anomaly from the predicted principal components $\mathbf{P}$ and corresponding spatial patterns $\mathbf{E}$. More details about the linear Markov model can be found in Chen and Yuan (2004) and Yuan et al. (2016).

The predictive skill at each grid point is assessed through cross-validated evaluation. We use the anomaly correlation (AC) to evaluate the predictive skill of the various experiments (Barnston et al., 2015; Li et al., 2020). To examine the significance of the AC difference between the sensitivity experiments and the control experiment, we use the Fisher's Z transformation to estimate the statistical significance of the difference of ACs (Solow, 1994; L. Wang et al., 2019). A detailed significance test of the correlation differences can be found in the Supporting Information S1. The potential predictability variance fraction (PPVF) is also calculated to measure the upper limit of predictive skill (see Supporting Information S1).

To test the sensitivity to the number of MEOF modes used in constructing the linear Markov model, the space averaged cross-validation predictive skill is calculated for the Ctrl experiment constructed for each number of MEOF modes (Figure S2 in Supporting Information S1). The 13-mode model presents a local peak of predictive skill, this model is chosen as a baseline because it has relatively high prediction skill and explains a reasonable fraction of the variance of the SIC anomaly (39% in Ctrl experiment) without introducing too much noise.

3. Results

3.1. Relationship Between September SIC and Surface Heat Fluxes

The local anomaly lag-correlations between net surface flux variables (NSSW, NSLW, NSHF), WV and CW in spring and September SIC at each grid point are calculated, which explicitly indicates the local atmosphere-ice interactions (Figure 1). A prominent feature in Figure 1 is the high correlation values in the Pacific and Siberian sectors of the Arctic (Beaufort, Chukchi, East Siberian and Laptev Seas), suggesting a significant contribution of the net surface heat absorption to the seasonal changes of SIC through humidity, clouds, and ice-albedo feedback (Choi et al., 2014; D. K. Perovich, Richter-Menge et al., 2008).

During March to April, the NSLW and NSHF exhibit negative correlations in the Pacific and Siberian sectors of the Arctic, while the correlation between NSSW and September SIC shows the opposite pattern. In the correlation with SICAs, WV and CW show spatial pattens similar to the NSHF, indicating the prominent role of the spring cloud water and water vapor on the September SICAs. In early spring, the NSHF is dominated by NSLW radiation. The NSSW is largely determined by cloudiness and water vapor, as the ocean is still largely covered by sea ice and thus has minimal surface albedo variations. In March and April, a positive anomaly of cloudiness and water vapor enhances the greenhouse effect and is associated with increased downward longwave radiation and decreased downward shortwave radiation. Thus, during March to April, the correlations between September SICA and NSLW are negative, whereas the NSSW correlations are positive (Kapsch et al., 2013, 2014).

In May, the NSSW and NSHF show negative correlation with September SIC in the marginal seas. This indicates that NSSW in the marginal seas surpasses NSLW and dominates the variation of NSHF in May. After the
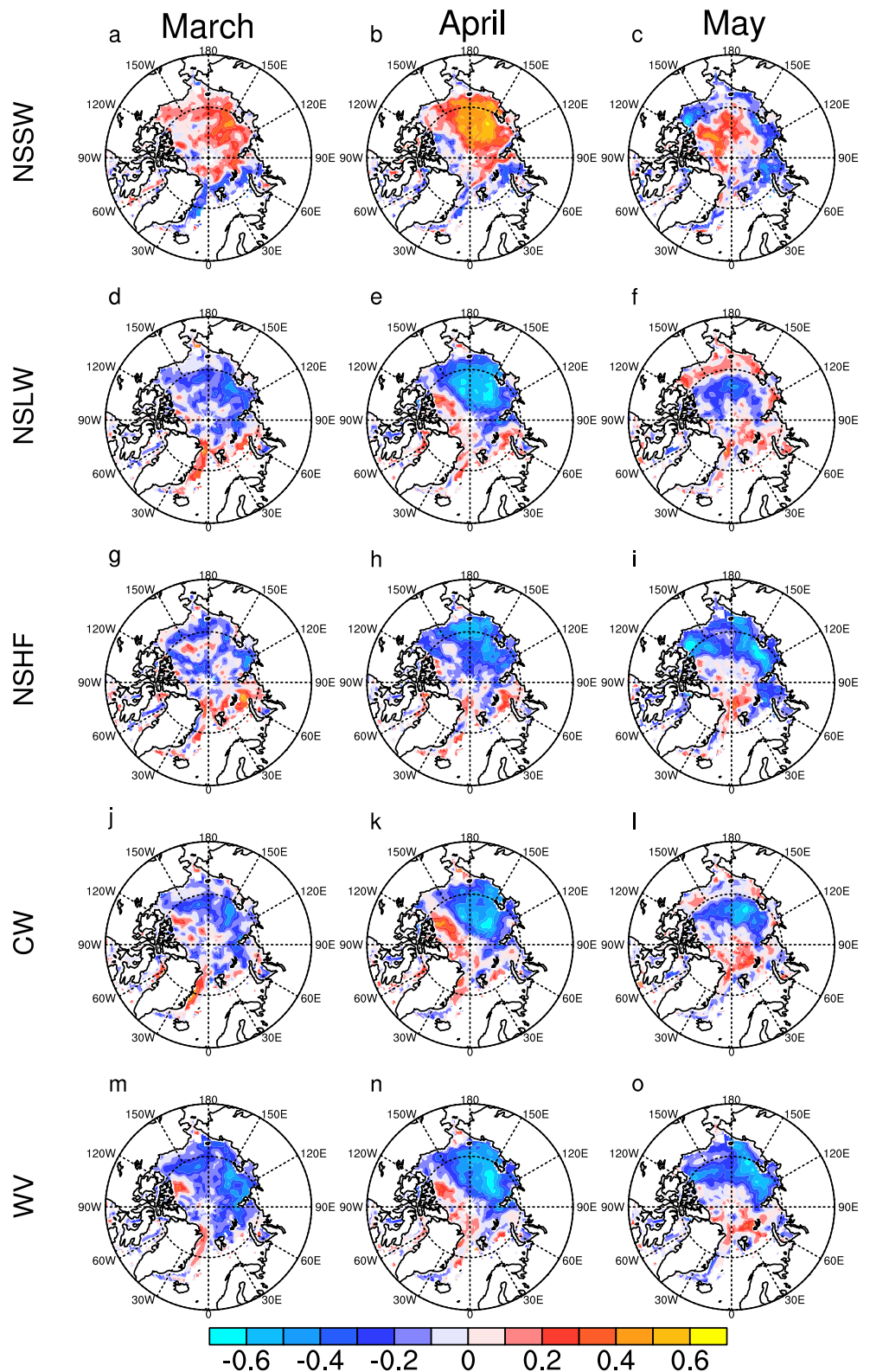
Figure 1. The anomaly correlations between five spring variables (NSSW, NSLW, NSHF, CW and WV) and September SIC from 1979 to 2019. From left to right are radiation fluxes (positive downward) in months of March, April, and May, from top to bottom are NSSW, NSLW, NSHF, CW and WV.
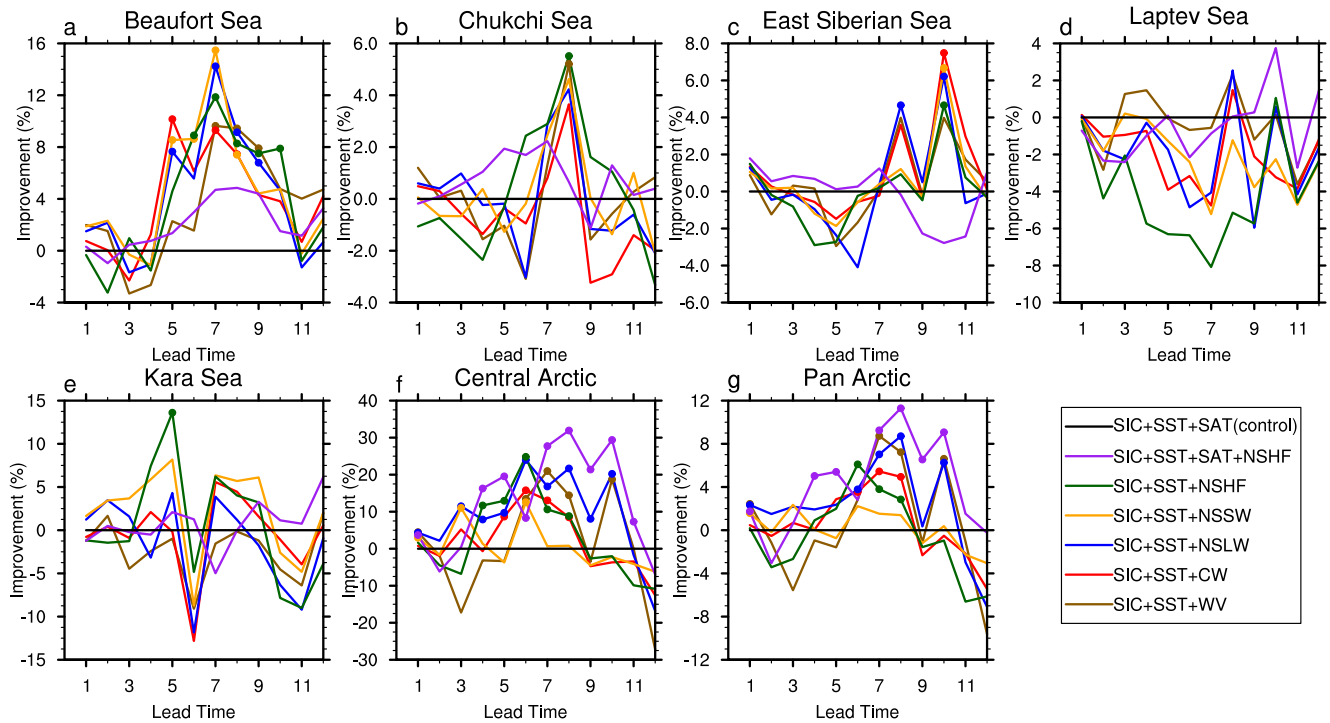
Figure 2. Improvement of predictive skill (AC) of September SIC in percentage of each experiment compared with control experiment as a function of lead months. The dots represent the difference between ACs that are significantly above the 95%.

melt onset, the surface albedo is lowered and more shortwave radiation is absorbed by the surface. A decreased surface albedo results in more shortwave radiation absorption, triggering a positive ice–albedo feedback and contributing to the accelerating ice retreat. The melt is amplified due to the ice albedo feedback which is reflected in significant negative correlations between September SICA and NSSW in the marginal seas during late spring (Kapsch et al., 2013, 2014). Thus, a better representation of thermodynamic processes in spring may improve the predictive skill of SIC in September. However, in the Atlantic sector of the Arctic, including the Greenland, Kara, and Barents Seas, the anomalies of surface heat fluxes are independent of WV and CW. The sea ice variability in this area likely has contributions from the inflow of warm Atlantic water (Smedsrud et al., 2013). The spatial correlation structures and values are broadly similar if the September SIC and spring predictor time series are both linearly detrended prior to computing the correlation (Figure S3 in Supporting Information S1). This suggest that the lagged relationships shown in Figure 1 are dominated by interannual variability rather than trends.

The variation of SICAs in September is highly correlated with NSSW in spring (Figure S4 in Supporting Information S1). The lag-correlation coefficient in Pan Arctic between NSSW in spring (March, April, May) and SICAs in September are −0.62, −0.63, −0.05, respectively (Table S1 in Supporting Information S1). The extreme low record of September SIC in 2012 is revealed to be influenced by the anomalously large solar absorption which developed in May (Babb et al., 2016). Similarly, the high SIC case in September 2013 and the low SIC case in September 2016 were associated with ice albedo feedback that was initialized by downwelling solar radiation over the open water (Babb et al., 2019; Kwok, 2018). With clear lag correlation between surface fluxes and SIC, we speculate that including surface fluxes in the Markov model will improve its prediction skill.

3.2. Skill of Predicting September Arctic SIC Anomalies

Figure 2 depicts the improvement of regional predictive skill of the seven sets of multivariate linear Markov models. The Arctic Ocean regions selected for analysis are shown in Figure S1 in Supporting Information S1. The regional SIC prediction skill values are spatially averaged over the six subregions. Moreover, to evaluate the predictive skill of the multivariate linear Markov models, we compare their skill to a potential predictability estimate and a persistence forecast, computed using the SICAs of the initial month as predictors of SICAs of the target month. The highest predictive skill appears in the Beaufort, Chukchi and East Siberian Seas, where ACs

can reach around 0.6 for 3-month lead when initialized in June. The forecast skill over these regions drops more slowly with lead time than over the Laptev, Kara Seas and Central Arctic. Thus, the SICAs in some marginal seas are predictable up to 3–4 months lead time, whereas the predictive skills in the Central Arctic and Kara Sea are fairly low with values below 0.5 (Figure S5 in Supporting Information S1). Because the Central Arctic is covered by sea ice with concentration close to 100%, the response of sea ice to the atmosphere and ocean is mainly reflected in ice thickness, not in SIC (Kwok & Rothrock, 2009).

The skill in predicting September SICAs in all models are superior to the skill of the persistence forecast at lead times longer than 2 months. This indicates that the short-term variation of September SICAs is largely influenced by the memory of SICAs itself, and the rapid decrease of predictive skills with lead time in persistence prediction highlights that the memory of SICAs is not enough to predict September sea ice beyond 2-month lead times. Therefore, the longer term September SICAs prediction should rely on other sources of memory. The PPVF is measured as the fraction of the total variability accounted for by the potentially predictable forced and internal source components. The variation of PPVF with regions is not as much as that of predictive skills. In regions of Pacific and Siberian sectors of the Arctic, the models can explain most of the potential predictability, while in Central Arctic, the variation explained by the models is far less than PPVF (Figure S6 in Supporting Information S1). This suggests remaining low-frequency intraseasonal fluctuations still include the chaotic, unpredictable fluctuations at monthly to seasonal timescale in Central Arctic.

Our results show that incorporating surface fluxes in statistical models improves the predictive skills over Pacific and Siberian sectors of the Arctic and Central Arctic when the models are initialized before June, whereas the improvements over Laptev Sea seem insignificant or degraded relative to Ctrl experiment (Figure 2, Figure S5 in Supporting Information S1). For instance, the surface fluxes and cloudiness lead to up 8%–15% improvement or degration in the predictive skill of September SIC relative to the control experiment in Beaufort Sea for lead times of 5–10 months. The model enhances the prediction skill for 7–8 months lead in Chukchi Sea, 8-10-month lead predictions in East Siberian Sea, 4–5 months lead predictions in Kara Sea, and 3 months lead predictions in Central Arctic. The improvement relative to the control experiment is 4%–6% in Chukchi Sea, 4%–8% in East Siberian Sea, 5%–15% in Kara Sea, and 10%–20% in Central Arctic. The prediction skill of the models which include longwave radiation, cloudiness and water vapor anomalies are lower than those which include shortwave radiation anomalies when the models are initialized in spring in Beaufort, Chukchi and East Siberian Seas (Figure 2, Figure S5 in Supporting Information S1). This may be due to the fact that shortwave absorption at the start of the melt season is strongly related to the date of melt onset, which may provide predictability for the September sea ice minimum via the ice-albedo feedback (Kapsch et al., 2014; Perovich et al., 2007; Schröder et al., 2014). The NSHF & SAT experiment, which include SIC, SST, SAT and NSHF information shows very limited improvements compared with other experiments, because of the counteraction during early spring between the net shortwave radiation and the net longwave flux. The experiments that include water vapor or cloudiness provide similar predictive skills (Figure 2, Figure S5 in Supporting Information S1). Their similar performance in the fitting period is a consequence of the physical connection between atmospheric variables.

Clearly, the statistical forecast schemes are sensitive to the choice of variables used to construct the models. Models that include surface flux terms may be more skillful at capturing short-term atmospheric perturbations that drive SIC variability. This result suggests that adding surface fluxes in a multivariate linear Markov model can improve the summer predictive skill and reduce the spring barrier for the Arctic sea ice prediction.

We next investigate the seasonality of the forecast skill in the multivariate linear Markov model. First, the seasonality of the persistence forecast skill constructed by SICAs is considered (Figure 3, row 1). The largest skill is seen over the marginal seas with predictable September SIC at lead times of up to 4 months, and minimal skill in the Central Arctic at lead times longer than 2 months. As shown in the first row of Figure 3, there is a consistent and significant drop in correlation coefficient between observed and predicted SIC when the predictions are initialized in boreal spring for Beaufort, Chukchi, East Siberian, Laptev, and Kara Seas.

The forecast skill of the multivariate linear Markov models exhibits strong seasonal dependence. The skill of predicting SIC using both SST and SAT anomalies as predictors is superior to the skill of the persistence forecast when the predictions are targeted in boreal summer and fall, which is most obvious over the marginal seas. Similar results are obtained when surface fluxes are used in the multivariate linear Markov model. Whether the models use only SIC, SST, and SAT, or include NSHF, NSLW, NSSW, CW and WV, forecasts are most skillful when initialized after June suggestive of a spring predictability barrier. This is also in line with the persistence
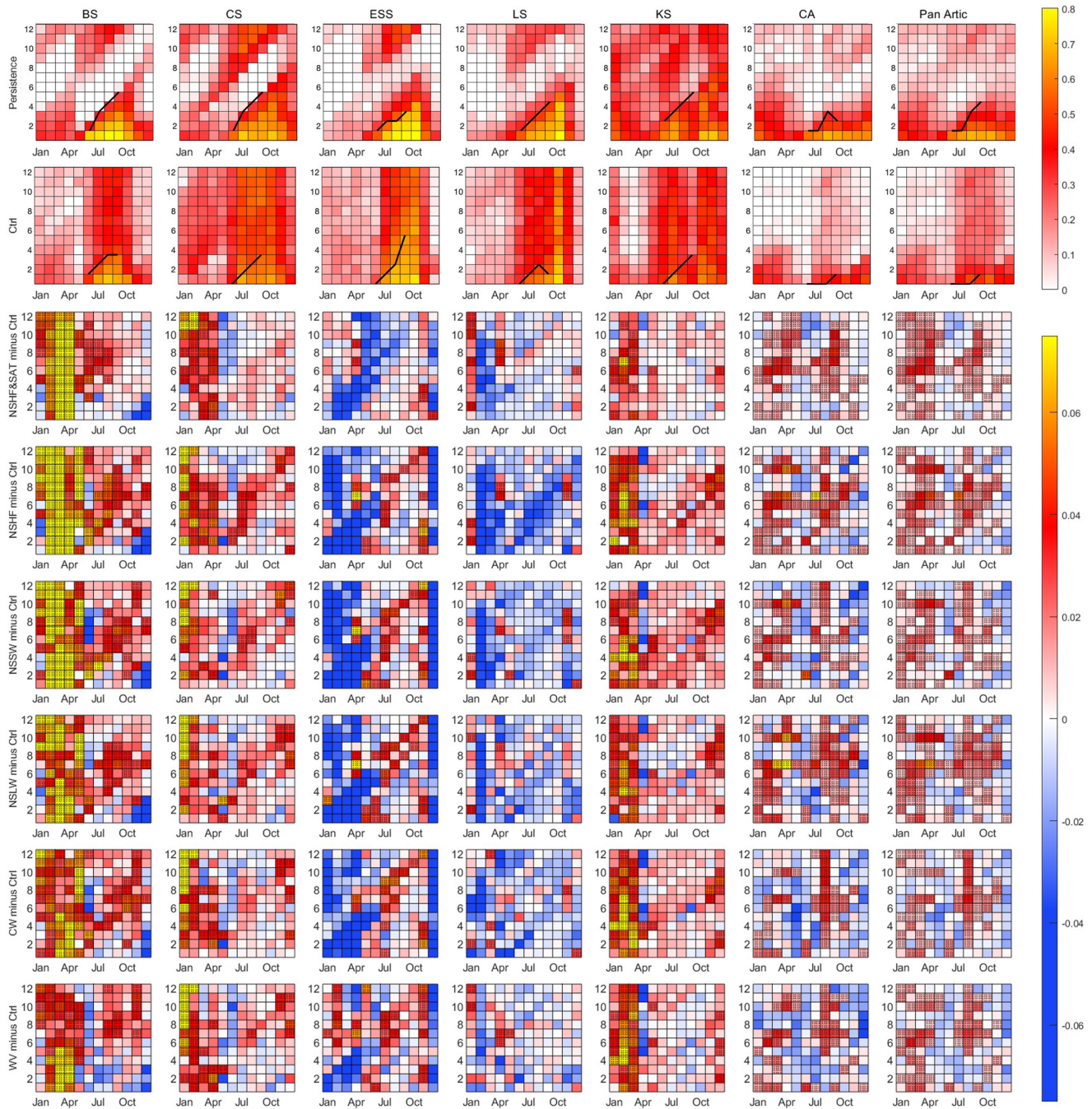
Figure 3. Skills (ACs) in predicting SICAs from 1979 to 2019 through cross-validation. The first two rows show the skills based on persistence forecast and Ctrl experiment (Color shading indicates the correlation). The black lines indicate the largest decorrelation between two lead months for June through September target months. The third to eighth rows show the improvement in the forecast skill between Ctrl experiment and NSHF & SAT, NSHF, NSSW and NSLW, CW and WV experiment (Color shading indicates the difference of AC between each experiment and ctrl experiment). The x axis represents target time and y axis represents lead time. The dotted grids indicate that the differences (improvements) are statistically significant at the 95% confidence interval.

forecast that also exhibits highest skill when initialized after June. The correlation coefficient between SICAs in spring and summer is extremely low for most regions, indicating the weak relationship between SICAs in spring and summer. This can partly explain the occurrence of a spring barrier in statistical models where SIC acts as the most important prediction variable.

According to the correlation coefficient of the Ctrl experiment, given the spatial and temporal sample sizes, a 0.025, 0.028, 0.024, 0.025, 0.026, 0.01 difference in Beaufort, Chukchi, East Siberian, Laptev, Kara Seas and

Central Arctic mean correlation coefficient is considered statistically significant at the 95% confidence level. The predictions starting in spring exhibit some modest improvements by considering surface fluxes, especially in the Beaufort, Chukchi and Kara Seas for NSHF, NSLW, NSSW, CW and WV experiments, and in the Central Arctic for NSHF & SAT and NSHF experiments (Figure 3), which are shown in over 4 (5)-month-lead when targeting September (October). The local thermodynamic processes appear to provide relatively large contributions to the total interannual SIC variability in the Beaufort, Chukchi, Kara Seas and Central Arctic. This holds some promise for enhanced predictability relative to persistence in these regions. Consistent with our results, Kapsch et al. (2014) presented that anomalies of spring downwelling longwave radiation play an important role in predicting summer SIC. Based on this information, our results show that the spring barrier can be reduced, but not eliminated, by using spring surface heat fluxes associated with clouds and water vapor in combination with SIC and SST. The forecasts with additional surface fluxes, cloudiness and water vapor data suggest that making use of the surface-atmosphere thermodynamics enhances the skill in predicting observed SIC over the Beaufort, Chukchi, Kara Seas and Central Arctic when the predictions are initialized in boreal spring at lead times of more than 5 months.

4. Summary

This study investigates the predictive skill of September Arctic SIC anomalies (SICAs) using a suite of multivariate linear Markov models. First, several sets of prediction experiments are constructed in a multivariate EOF space of observed SIC, SST, and SAT spanning 1979–2019 as the control experiment, then adding different combinations of cloudiness, water vapor and surface heat flux variables (NSHF, NSLW and NSSW). The control experiment shows limited September SICAs forecast skill initialized before June when only using SIC, SST, and SAT data as predictors.

The local lag-correlations between September SICAs and spring surface heat flux anomalies suggest that the local spring atmosphere-ice interactions plays a significant role in the Pacific sector of the Arctic sea ice variability. We find that considering the surface fluxes helps to improve the representation of the thermodynamics associated with water vapor and cloudiness anomalies in spring over the marginal seas and eventually leads to the higher predictive skill of the SICAs relative to the control experiment. In particular, the NSHF, NSSW and NSLW experiments show enhanced predictive skill in Beaufort, Chukchi, Kara Seas and Central Arctic. For instance, adding spring NSSW leads up 10%–15% improvement in the predictive skill of September SIC in Beaufort and Kara Seas, and up to 20% improvement in Central Arctic for lead times of 3 months when initialized before June. This suggests that using the atmosphere-ice thermodynamics, in the form of surface heat flux variables, clouds and water vapor enhances the skill in predicting September SICAs when initialized before June.

It should be noted that there are still uncertainties with our analysis since the SIC data is retrieved from satellite-observed passive microwave brightness temperature data, and the atmospheric temperature and surface flux data are from reanalysis products. However, this study shows that the spring barrier for the Arctic sea ice concentration prediction can be somewhat reduced by improving the surface heat budget in a multivariate linear Markov model.

Data Availability Statement

All data used here are open accessed. The monthly sea ice concentrations (SIC) data is downloaded from National Snow & Ice Data Center https://nsidc.org/data/NSIDC-0081/versions/1 (last access: August 2021). The sea surface temperature (SST) data is downloaded from Met Office Hadley Centre observation datasets https://www.metoffice.gov.uk/hadobs/hadisst/data/download.html. The NCEP-DOE Reanalysis 2 surface air temperature data (SAT) is available at https://psl.noaa.gov/data/gridded/data.ncep.reanalysis2.gaussian.html. The ERA5 net surface shortwave radiation, net surface longwave radiation, surface latent heat flux and surface sensible heat flux are all downloaded from https://cds.climate.copernicus.eu/cdsapp#!/dataset/reanalysis-era5-single-levels-monthly-means?tab=form.

References

Babb, D. G., Landy, J. C., Barber, D. G., & Galley, R. J. (2019). Winter sea ice export from the Beaufort Sea as a preconditioning mechanism for enhanced summer melt: A case study of 2016. *Journal of Geophysical Research: Oceans*, *124*(9), 6575–6600. https://doi.org/10.1029/2019JC015053

Babb, D. G., Galley, R. J., Barber, D. G., & Rysgaard, S. (2016). Physical processes contributing to an ice free Beaufort Sea during September 2012. *Journal of Geophysical Research (Oceans)*, *121*(1), 267–283. https://doi.org/10.1002/2015JC010756

Ballinger, T. J., Overland, J. E., Wang, M., Bhatt, U. S., Hanna, E., Hanssen-Bauer, I., et al. (2020). Arctic report card 2020: Surface air temperature. https://doi.org/10.25923/gcw8-2z06

Barnston, A. G., Tippett, M. K., van den Dool, H. M., & Unger, D. A. (2015). Toward an improved multimodel ENSO prediction. *Journal of Applied Meteorology and Climatology*, *54*(7), 1579–1595. https://doi.org/10.1175/JAMC-D-14-0188.1

Bonan, D. B., Bushuk, M., & Winton, M. (2019). A spring barrier for regional predictions of summer Arctic Sea Ice. *Geophysical Research Letters*, *46*(11), 5937–5947. https://doi.org/10.1029/2019GL082947

Brunette, C., Tremblay, B., & Newton, R. (2019). Winter coastal divergence as a predictor for the minimum sea ice extent in the Laptev Sea. *Journal of Climate*, *32*(4), 1063–1080. https://doi.org/10.1175/JCLI-D-18-0169.1

Bushuk, M., Winton, M., Bonan, D. B., Blanchard-Wrigglesworth, E., & Delworth, T. L. (2020). A mechanism for the Arctic sea ice spring predictability barrier. *Geophysical Research Letters*, *47*(13), e2020GL088335. https://doi.org/10.1029/2020GL088335

Chen, D., & Yuan, X. (2004). A Markov model for seasonal forecast of Antarctic sea ice. *Journal of Climate*, *17*(16), 3156–3168. https://doi.org/10.1175/1520-0442(2004)017<3156:AMMFSF>2.0.CO;2

Choi, Y. S., Kim, B. M., Hur, S. K., Kim, S. J., Kim, J. H., & Ho, C. H. (2014). Connecting early summer cloud-controlled sunlight and late summer sea ice in the Arctic. *Journal of Geophysical Research*, *119*(19), 11087–11099. https://doi.org/10.1002/2014JD022013

Comiso, J. C. (2017). Bootstrap Sea ice concentrations from Nimbus-7 SMMR and DMSP SSM/I-SSMIS, version 3.

Drobot, S. D. (2007). Using remote sensing data to develop seasonal outlooks for Arctic regional sea-ice minimum extent. *Remote Sensing of Environment*, *111*(2–3), 136–147. https://doi.org/10.1016/j.rse.2007.03.024

Drobot, S. D., & Maslanik, J. A. (2002). A practical method for long-range forecasting of ice severity in the Beaufort Sea. *Geophysical Research Letters*, *29*(8), 54-1–54-4. https://doi.org/10.1029/2001GL014173

Emmerson, C., & Lahn, G. (2012). Arctic opening: Opportunity and risk in the high North. Retrieved from http://www.alaskadispatch.com/article/

Guemas, V., Doblas-Reyes, F. J., Mogensen, K., Keeley, S., & Tang, Y. (2014). Ensemble of sea ice initial conditions for interannual climate predictions. *Climate Dynamics*, *43*(9), 2813–2829. https://doi.org/10.1007/s00382-014-2095-7

Hersbach, H., Bell, B., Berrisford, P., Hirahara, S., Horányi, A., Muñoz-Sabater, J., et al. (2020). The ERA5 global reanalysis. *Quarterly Journal of the Royal Meteorological Society*, *146*(730), 1999–2049. https://doi.org/10.1002/qj.3803

Jung, T., Gordon, N. D., Bauer, P., Bromwich, D. H., Chevallier, M., Day, J. J., et al. (2016). Advancing polar prediction capabilities on daily to seasonal time scales. *Bulletin of the American Meteorological Society*, *97*(9), 1631–1647. https://doi.org/10.1175/BAMS-D-14-00246.1

Kalnay, E., Kanamitsu, M., Kistler, R., Collins, W., Deaven, D., Gandin, L., et al. (1996). The NCEP/NCAR 40-year reanalysis project. *Bulletin of the American Meteorological Society*, *77*(3), 437–472. https://doi.org/10.1175/1520-0477(1996)077<0437:TNYRP>2.0.CO;2

Kapsch, M. L., Graversen, R. G., Economou, T., & Tjernström, M. (2014). The importance of spring atmospheric conditions for predictions of the Arctic summer sea ice extent. *Geophysical Research Letters*, *41*(14), 5288–5296. https://doi.org/10.1002/2014GL060826

Kapsch, M.-L., Graversen, R. G., & Tjernström, M. (2013). Springtime atmospheric energy transport and the control of Arctic summer sea-ice extent. *Nature Climate Change*, *3*(8), 744–748. https://doi.org/10.1038/nclimate1884

Kistler, R., Collins, W., Saha, S., White, G., Woollen, J., Kalnay, E., et al. (2001). The NCEP–NCAR 50–year reanalysis: Monthly means CD–ROM and documentation. *Bulletin of the American Meteorological Society*, *82*(2), 247–267. https://doi.org/10.1175/1520-0477(2001)082<0247:TNNYRM>2.3.CO;2

Kwok, R. (2018). Arctic sea ice thickness, volume, and multiyear ice coverage: Losses and coupled variability (1958-2018). *Environmental Research Letters*, *13*(10), 105005. https://doi.org/10.1088/1748-9326/AAE3EC

Kwok, R., & Rothrock, D. A. (2009). Decline in Arctic sea ice thickness from submarine and ICESat records: 1958-2008. *Geophysical Research Letters*, *36*(15). https://doi.org/10.1029/2009gl039035

Lenetsky, J. E., Tremblay, B., Brunette, C., & Meneghello, G. (2021). Subseasonal predictability of Arctic Ocean sea ice conditions: Bering Strait and Ekman-driven ocean heat transport. *Journal of Climate*, *34*(11), 4449–4462. https://doi.org/10.1175/JCLI-D-20-0544.1

Li, X., Bordbar, M. H., Latif, M., Park, W., & Harlaß, J. (2020). Monthly to seasonal prediction of tropical Atlantic sea surface temperature with statistical models constructed from observations and data from the Kiel Climate Model. *Climate Dynamics*, *54*(3–4), 1829–1850. https://doi.org/10.1007/s00382-020-05140-6

Lindsay, R. W., Zhang, J., Schweiger, A. J., & Steele, M. A. (2008a). Seasonal predictions of ice extent in the Arctic Ocean. *Journal of Geophysical Research*, *113*(C2), C02023. https://doi.org/10.1029/2007JC004259

Lindsay, R. W., Zhang, J., Schweiger, A. J., & Steele, M. A. (2008b). Seasonal predictions of ice extent in the Arctic Ocean. *Journal of Geophysical Research*, *113*(C2), C02023. https://doi.org/10.1029/2007JC004259

Liu, J., Song, M., Horton, R. M., & Hu, Y. (2015). Revisiting the potential of melt pond fraction as a predictor for the seasonal Arctic sea ice extent minimum. *Environmental Research Letters*, *10*(5), 054017. https://doi.org/10.1088/1748-9326/10/5/054017

Melia, N., Haines, K., & Hawkins, E. (2016). Sea ice decline and 21st century trans-Arctic shipping routes. *Geophysical Research Letters*, *43*(18), 9720–9728. https://doi.org/10.1002/2016GL069315

Onarheim, I. H., Eldevik, T., Årthun, M., Ingvaldsen, R. B., & Smedsrud, L. H. (2015). Skillful prediction of Barents Sea ice cover. *Geophysical Research Letters*, *42*(13), 5364–5371. https://doi.org/10.1002/2015GL064359

Perovich, D., Meier, W., Tschudi, M., Hendricks, S., Petty, A. A., Divine, D., et al. (2020). Arctic report card 2020: Sea ice. https://doi.org/10.25923/n170-9h57

Perovich, D. K., Nghiem, S. V., Markus, T., & Schweiger, A. (2007). Seasonal evolution and interannual variability of the local solar energy absorbed by the Arctic sea ice-ocean system. *Journal of Geophysical Research*, *112*(3), 1–13. https://doi.org/10.1029/2006JC003558

Perovich, D. K., Richter-Menge, J. A., Jones, K. F., & Light, B. (2008). Sunlight, water, and ice: Extreme Arctic sea ice melt during the summer of 2007. *Geophysical Research Letters*, *35*(11), L11501. https://doi.org/10.1029/2008GL034007

Petty, A. A., Schröder, D., Stroeve, J. C., Markus, T., Miller, J., Kurtz, N. T., et al. (2017). Skillful spring forecasts of September Arctic sea ice extent using passive microwave sea ice observations. *Earth's Future*, *5*(2), 254–263. https://doi.org/10.1002/2016EF000495

Rantanen, M., Karpechko, A. Y., Lipponen, A., Nordling, K., Hyvärinen, O., Ruosteenoja, K., et al. (2022). The Arctic has warmed nearly four times faster than the globe since 1979. *Communications Earth & Environment*, *3*(1), 168. https://doi.org/10.1038/s43247-022-00498-3

Schröder, D., Feltham, D. L., Flocco, D., & Tsamados, M. (2014). September Arctic sea-ice minimum predicted by spring melt-pond fraction. *Nature Climate Change*, *4*(5), 353–357. https://doi.org/10.1038/nclimate2203

Sigmond, M., Fyfe, J. C., Flato, G. M., Kharin, V. V., & Merryfield, W. J. (2013). Seasonal forecast skill of Arctic sea ice area in a dynamical forecast system. *Geophysical Research Letters*, *40*(3), 529–534. https://doi.org/10.1002/grl.50129

Smedsrud, L. H., Esau, I., Ingvaldsen, R. B., Eldevik, T., Haugan, P. M., Li, C., et al. (2013). The role of the Barents Sea in the Arctic climate system. *Reviews of Geophysics*, *51*(3), 415–449. https://doi.org/10.1002/rog.20017

Solow, A. R. (1994). 22 Statistical methods in atmospheric science. *Environmental Statistics*, *12*, 717–734. https://doi.org/10.1016/S0169-7161(05)80024-0

Stroeve, J., Hamilton, L. C., Bitz, C. M., & Blanchard-Wrigglesworth, E. (2014). Predicting September sea ice: Ensemble skill of the SEARCH sea ice outlook 2008-2013. *Geophysical Research Letters*, *41*(7), 2411–2418. https://doi.org/10.1002/2014GL059388

Walsh, J. E., Stewart, J. S., & Fetterer, F. (2019). Benchmark seasonal prediction skill estimates based on regional indices. *The Cryosphere*, *13*(4), 1073–1088. https://doi.org/10.5194/tc-13-1073-2019

Wang, L., Yuan, X., & Li, C. (2019). Subseasonal forecast of Arctic sea ice concentration via statistical approaches. *Climate Dynamics*, *52*(7–8), 4953–4971. https://doi.org/10.1007/s00382-018-4426-6

Wang, L., Yuan, X., Ting, M., & Li, C. (2016). Predicting summer Arctic sea ice concentration intraseasonal variability using a vector autoregressive model. *Journal of Climate*, *29*(4), 1529–1543. https://doi.org/10.1175/JCLI-D-15-0313.1

Wang, Y., Yuan, X., Bi, H., Bushuk, M., Liang, Y., Li, C., & Huang, H. (2022). Reassessing seasonal sea ice predictability of the Pacific-Arctic sector using a Markov model. *The Cryosphere*, *16*(3), 1141–1156. https://doi.org/10.5194/tc-16-1141-2022

Wang, Y., Yuan, X., & Cane, M. A. (2022). Coupled mode of cloud, atmospheric circulation, and sea ice controlled by wave-3 pattern in Antarctic winter. *Environmental Research Letters*, *17*(4), 044053. https://doi.org/10.1088/1748-9326/ac5272

Williams, J., Tremblay, B., Newton, R., & Allard, R. (2016). Dynamic preconditioning of the minimum september seasea-ice extent. *Journal of Climate*, *29*(16), 5879–5891. https://doi.org/10.1175/JCLI-D-15-0515.1

Yuan, X., Chen, D., Li, C., Wang, L., & Wang, W. (2016). Arctic sea ice seasonal prediction by a linear Markov model. *Journal of Climate*, *29*(22), 8151–8173. https://doi.org/10.1175/JCLI-D-15-0858.1